

Accepted Manuscript

Structure-activity relationships in fungal nucleobases transporters as dissected by the inhibitory effects of novel purine analogues

Efthymios-Spyridon Gavriil, Spyridon Dimitrakis, Georgia Papadaki, Sophia Balaska, George Lambrinidis, Nikolaos Lougiakis, Panagiotis Marakos, George Diallinas, Nicole Pouli, Emmanuel Mikros

PII: S0223-5234(18)30529-4

DOI: [10.1016/j.ejmech.2018.06.038](https://doi.org/10.1016/j.ejmech.2018.06.038)

Reference: EJMECH 10508

To appear in: *European Journal of Medicinal Chemistry*

Received Date: 7 March 2018

Revised Date: 13 June 2018

Accepted Date: 13 June 2018

Please cite this article as: E.-S. Gavriil, S. Dimitrakis, G. Papadaki, S. Balaska, G. Lambrinidis, N. Lougiakis, P. Marakos, G. Diallinas, N. Pouli, E. Mikros, Structure-activity relationships in fungal nucleobases transporters as dissected by the inhibitory effects of novel purine analogues, *European Journal of Medicinal Chemistry* (2018), doi: 10.1016/j.ejmech.2018.06.038.

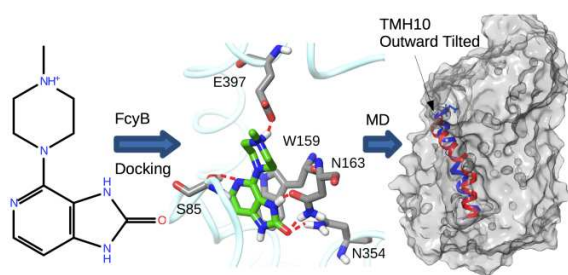
This is a PDF file of an unedited manuscript that has been accepted for publication. As a service to our customers we are providing this early version of the manuscript. The manuscript will undergo copyediting, typesetting, and review of the resulting proof before it is published in its final form. Please note that during the production process errors may be discovered which could affect the content, and all legal disclaimers that apply to the journal pertain.



Structure-activity relationships in fungal nucleobases transporters as dissected by the inhibitory effects of novel purine analogues

Efthymios-Spyridon Gavriil,^a Spyridon Dimitrakis,^a Georgia Papadaki,^b Sophia Balaska,^b George Lambrinidis,^a Nikolaos Lougiakis,^a Panagiotis Marakos,^a George Diallinas^{*,b}, Nicole Pouli,^a Emmanuel Mikros^{*,a}

Graphical abstract



Structure-activity relationships in fungal nucleobases transporters as dissected by the inhibitory effects of novel purine analogues

Efthymios-Spyridon Gavriil,^a Spyridon Dimitrakis,^a Georgia Papadaki,^b Sophia Balaska,^b George Lambrinidis,^a Nikolaos Lougiakis,^a Panagiotis Marakos,^a George Diallinas*^b, Nicole Pouli,^a Emmanuel Mikros*^a

^a *Division of Pharmaceutical Chemistry, Department of Pharmacy, National and Kapodistrian University of Athens, Panepistimiopolis, Zografou 15771, Greece.*

^b *Department of Biology, National and Kapodistrian University of Athens, Panepistimiopolis, Athens 15784, Greece.*

*Correspondence to:

Emmanuel Mikros, e-mail: mikros@pharm.uoa.gr

George Diallinas, e-mail: diallina@biol.uoa.gr

Abstract

We have previously rationally designed, synthesized and tested a number of 3-deazapurine analogues, which inhibit the ubiquitous fungal nucleobase transporter FcyB, through binding in its major substrate binding site, by specifically interacting with Asn163. Here, in an effort to further understand the molecular details of structure-activity relationships in all three major nucleobase transporters of fungi, we extend this study by designing, based on our previous experience, synthesizing and testing further 3-deazapurine analogues. We thus identify seven new compounds with relatively high affinity (19-106 μ M) for the FcyB binding site. Importantly, four of these compounds can also efficiently inhibit AzgA, a structurally and evolutionary distinct, but functionally similar, purine transporter. Contrastingly, none of the new compounds tested had any effect on the transport activity of the uric acid-xanthine transporter UapA, albeit this being a structural homologue of AzgA. Besides the apparent importance for understanding how nucleobase transporter specificity is determined at the molecular level, our work might constitute a critical step in the design of novel purine-related antifungals.

Key words: purine isosters / imidazo[4,5-c]pyridine / rational design / *Aspergillus nidulans* / purine transporters / Molecular Dynamics

1. INTRODUCTION

Early genetic and biochemical studies established the presence of highly specific nucleobase transporters in fungi. The lack of growth on purines or the use of purine or pyrimidine toxicity, caused either by an excess of a base (e.g. uracil, uric acid), or by a cytotoxic analogue (e.g. oxypurinol, allopurinol, 8-azaguanine, 5-fluorouracil, 5-fluorocytosine), provided a powerful tool to select mutants and identify the corresponding genes.[1,2] Out of work performed mostly in *Aspergillus nidulans*, but also in *Aspergillus fumigatus*, *Saccharomyces cerevisiae* and *Candida albicans*, we now know that there are four specific nucleobase uptake systems that belong to two structurally and evolutionary distinct protein families.[3] The first, called NAT (Nucleobase Ascorbate Transporters, also called Nucleobase Cation Symporters 2 or NCS2) includes two sub-groups, with totally non-overlapping specificities, the UapA/C-like and the AzgA-like transporters.[4-6] UapA/C transporters are specific for uric acid and xanthine, whereas AzgA transporters are specific for adenine-hypoxanthine-guanine. In addition, UapA/C and AzgA transport totally different purine analogues and drugs, namely oxypurinol and allopurinol versus 8-azaguanine and 6-mercaptopurine, respectively. The second major family is called NCS1 (Nucleobase Cation Symporters 1) and also includes two sub-groups with totally non-overlapping specificities, the Fcy-like [7,8] and the Fur-like transporters.[9,10] Fcy-like transporters are specific for adenine-hypoxanthine-guanine-cytosine, whereas Fur-like transporters are highly specific for either uracil or allantoin, the latter being a purine catabolic metabolite. All these transporter groups function as H⁺-dependent secondary transporters or H⁺ symporters. All filamentous fungi, including the major pathogens, *A. fumigatus* and *A. flavus*, possess all four subgroups of the two families, while several yeasts, including *S. cerevisiae*, lack the UapA/C subgroup.³ The distinction of nucleobase transporters in two major families, initially based simply on functional assays, was confirmed by structural approaches, including x-ray crystallography and relative modeling approaches of bacterial homologues,[11-15] but also of the UapA transporter of *A. nidulans*. [16] The sub-group distinction of the NAT and NCS1 families is supported by prominent differences in their substrate specificities and the presence of characteristic amino acid sequence motifs.

What seems to be an apparent paradox is that while UapA and AzgA are structurally similar (NAT family), they transport entirely different substrates and drugs, while FcyB which belong to a different major family (NCS1) has very similar specificity profile and similar binding affinities for purines with AzgA. The only rigorous way to functionally distinguish AzgA from FcyB is via their relative capacity to transport cytosine or specific purine or pyrimidine analogues. These observations suggest that the architecture of the binding site of NAT and NCS1 transporter is shaped via both divergent and convergent evolution events. While functional details for substrate binding and transport have been elucidated by genetic and *in vivo* transport kinetic approaches for several fungal members of the NCS1 family (see references above), direct structural information comes only from the bacterial benzylhydantoin Mhp1 transporter.[12-14] Mhp1, but also all studied fungal NCS1 homologues modeled on the Mh1 structure, are characterized by a core of ten transmembrane helices divided in two symmetric sets oppositely orientated with respect to the membrane, termed the 5-helix inverted repeat (SHIR) motif. There are additionally two C-terminal transmembrane helices (TMH11 and TMH12), which apparently do not participate in transport activity, and their role is unknown. Importantly, as the structure of Mhp1 has been previously solved in three different

conformations, this has provided insights into the molecular basis of the alternating access mechanism of transport. Briefly, sodium ions bind and favor the formation of an outward-facing state and the consequent substrate binding in a cavity formed between a “bundle” (TMHs 1, 2, 6 and 7) and a “hash” motif (TMHs 3, 4, 8 and 9). Upon substrate binding TMH10 bends over the substrate in the occluded state triggering the rotation of the one motif relative to the other towards the inward-facing conformation, accompanied by a bend of TMH5 which opens the cavity further to the intracellular and enables substrate transport.

In *A. nidulans* we have developed tools to study rigorously structure-function relationships in nucleobase transporters. These include the construction of strains expressing a single nucleobase transporter in a genetically ‘clean’ background lacking all functionally similar transporters due to multiple null mutations, and efficient cellular and functional assays measuring transporter expression, turnover and activity.[17, 18] Additionally, all nucleobase transporters of *A. nidulans* have been extensively analyzed via classical and reverse genetics and modeling using available crystal structures of bacterial homologues.[18] Thus, we have defined, at the molecular level, transporter-substrate interactions and identified the major elements of substrate binding sites. Furthermore, we have identified elements located outside the major binding site that affect nucleobase transporter specificity, collectively named gating elements.[17-19] Most importantly, we obtained direct evidence of structure-function relationships in UapA by analyzing the crystal structure of a genetically stabilized version of UapA in complex with xanthine.[19] The crystal structure validated conclusions drawn by genetic and biochemical approaches and further showed dimerization is critical for UapA function and specificity.[16-18]

In a different but complementary approach, we recently developed chemical biology methodologies to better understand how specificity is determined in different nucleobase transporters.[20] In particular, we used a virtual screening and semi-rational approaches to identify compounds that might interact with the substrate binding site of a specific nucleobase transporter, and then test whether positive-scoring compounds can also be recognized by a functionally similar transporter. More specifically, we looked for FcyB ligands and then tested whether they interact with AzgA (i.e. a functional analogue) or UapA (i.e. a structural homologue). We thus identified a number of 3-deazapurines substituted in the corresponding 6- and 9-positions of the original purine scaffold, which proved highly specific solely for FcyB.[20] One of these compounds proved to be moderately toxic for *A. nidulans* growth. In the present work, we exploited findings of our original approach to identify further purine analogues that might act differentially on the relative *A. nidulans* transporters. We identified seven new compounds recognized with high affinity by the FcyB, and among them, four were also recognized by AzgA, but none by UapA. This work complements in our understanding of the transporter-substrate interactions and could also be considered as an important step towards developing purine-related analogues as potentially novel highly targeted antifungals.

2. RESULTS

2.1. Rationale for 3-deazapurine analogue design. In order to design new chemical probes allowing better understanding the FcyB function, a structural model for the protein was required. In this study we have de novo constructed an FcyB structure by homology modeling, using as template the most recent Mhp1 occluded crystal structure (pdb 4d1d), which is in the outward conformation in complex with an hydantoin derivative acting as inhibitor.[13] The new model displays only few

differences within the binding cavity of the transporter when compared to a previously constructed model based on the occluded Mhp1 topology (pdb 2jlo).[7] The integrity of the transmembrane helices is improved when compared with the previous model. The major difference is related to the first part of TMH10 between Glu401 and Tyr409, which is tilted moving away from the cavity forming the outward conformation. For exploring possibilities of modifying further the 3-deazapurine scaffold, we were guided by the structure-activity relationships of the recently reported series of 1,4-substituted-3-deazapurine analogues,[20] which can be summarized as follows. The most potent analogue has been found to be the 4-benzylamine substituted derivative **1** (**Figure 1A**), interacting with Glu397 on TMH9-10 at the edge of the transporter outward cavity along with the main interaction between N3 and Asn163.

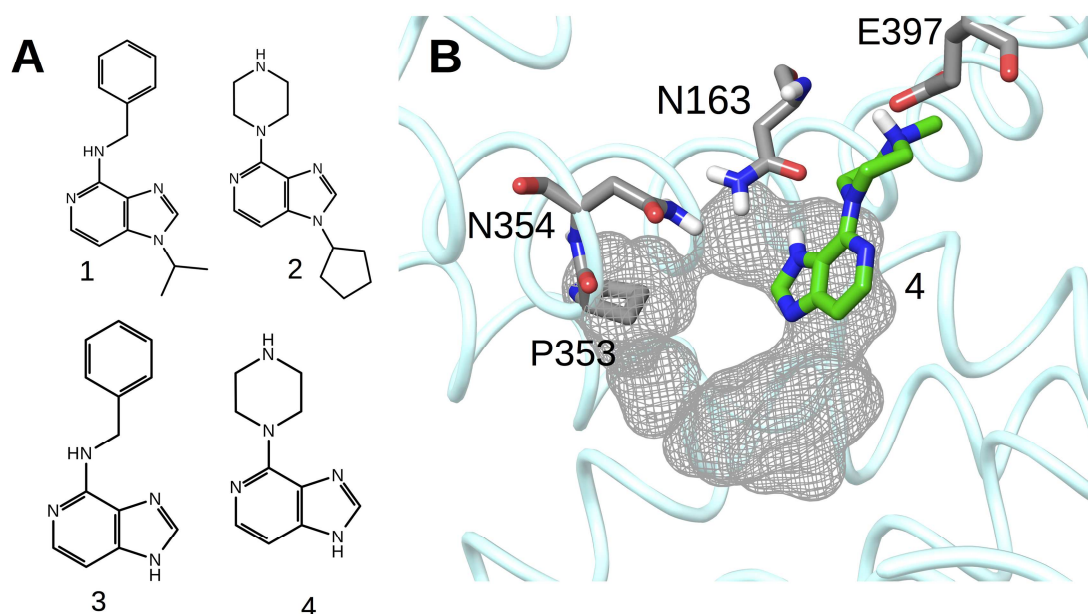


Figure 1. A. Structures of Compounds 1-4. **B.** Global minimum energy structure of compound 4 in complex with FcyB model. In grey the hydrophobic surface of the protein binding pocket near Pro353 forming a cavity that is targeted by the synthesized compounds.

Additionally, compound **2** bearing at position 4- a methylpiperazino- group, containing a quaternary nitrogen positively charged at the physiological pH conditions, has proved to possess interesting activity as well. The corresponding monosubstituted parent analogues **3** and **4** respectively (**Figure 1A**), albeit not highly potent, maintain a certain degree of inhibitory activity against both AzgA and FcyB. In order to further investigate the different substitutions of this scaffold, we examined the possibilities for an additional interaction with an important residue in the vicinity, namely Asn354 by introducing at position 2- an enolic OH or SH group, maintaining the optimum substitution pattern at position 4-. With the aim of facilitating the interpretation of the resulting data, we have decided to preserve only the 4-substituent of the previously studied compounds, and thus deal with 2,4-disubstituted analogues. This would also provide the possibility to investigate the effect of both imidazole nitrogen atoms in the molecular level. Furthermore, no substitution at position 1- together with the enolic OH at position 2- which is expected to be in its carbonyl form

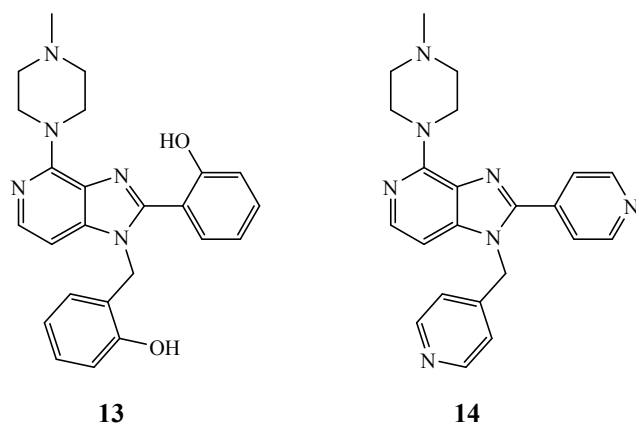


Figure 2. Structure of compounds **13-14**

2.3 Evaluation of novel 3-deazapurine analogues as inhibitors of purine transporters. The new 3-deazapurine analogues were tested as competitive inhibitors of FcyB- or AzgA-mediated ^3H -radiolabelled adenine uptake, or UapA-mediated ^3H -radiolabelled xanthine uptake. In all cases, assays were performed, as already described,[22] in strains expressing the specific transporter studied in the absence of other transporters of similar specificity.[20] The competition results for FcyB and AzgA are summarized in **Figure 3**, along with the previously reported compounds **3** and **4**, as well as, unlabeled adenine or hypoxanthine (physiological substrates of FcyB and AzgA), as controls.

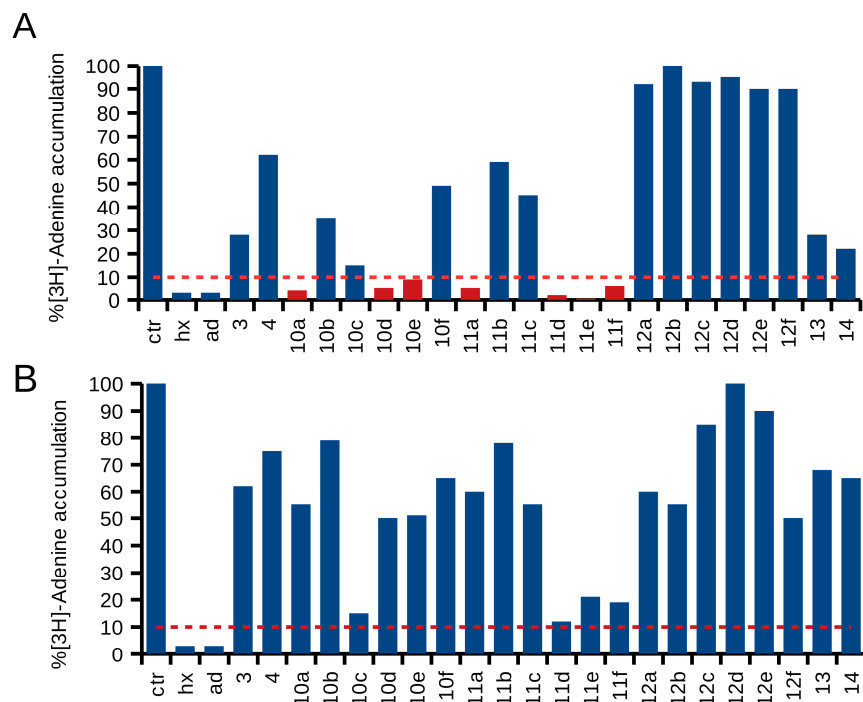


Figure 3. Competition of FcyB- (A) or AzgA- (B) mediated [^3H]-adenine uptake by 1000-fold excess (0.5 mM) of unlabeled 3-deazapurine analogues.

Compounds **12a-f**, **13** and **14** did not show any inhibitory activity. Among the designed derivatives, **10a**, **10d**, **10e**, **11d**, **11e** and **11f** reduced FcyB-mediated ^3H -adenine accumulation rate to <10%, compared to the control (absence of any inhibitor). The compounds **10c**, **11d**, **11e** and **11f** also showed a relative significant

inhibition of AzgA-mediated ^3H -adenine accumulation rate, which however was lower than the one observed with FcyB. None of the compounds tested showed any inhibitory activity on UapA-mediated transport of xanthine (data not shown).

2.4 Kinetic characterization of competing analogues Compounds that proved to be active as inhibitors of FcyB were further evaluated by estimating their K_i , using IC_{50} measurements. Results are shown in **Table 1**. All compounds exhibited values lower than $110\ \mu\text{M}$ for FcyB, with the methylpiperazine analogue **10a** being the most potent followed by the benzylamine analogue **11e**, exhibiting K_i of 19 and $42\ \mu\text{M}$ respectively. As compound **11d** showed the higher inhibitory activity against AzgA the corresponding K_i value was also determined and found to be $58\ \mu\text{M}$.

Table 1. 3-deazapurine analogue binding profile of FcyB

Compound	K_i (μM)
10a	19 ± 3
10c	106 ± 12
10d	49 ± 10
10e	100 ± 5
11a	74 ± 6
11d	82 ± 8
11f	72 ± 4
11e	42 ± 6
1	5 ± 1
2	38 ± 6
Adenine	7 ± 1
Hypoxanthine	11 ± 1

Results are averages of at least three independent experiments with three replicates for each concentration point. SD was $< 10\%$.

2.5 Molecular Modeling FcyB-ligand interactions In order to further develop a structure-activity relationship model and gain insight in FcyB-ligand interactions, MD and docking calculations have been carried out. First, we present the models derived by docking calculations for the most active compounds namely compounds **10a** and **11e**. Each one of these two compounds contains different substitutions at positions 4- and 2- thus exemplifying the basic characteristics for the protein-ligand interactions as derived by theoretical calculations. The synthesized analogues were submitted to docking calculations using the Induced Fit Docking algorithm as implemented in Maestro 10 (Schrodinger Inc). The most active compound the piperazine-substituted **10a** was considered as positively charged, since the pK_a value of N-methylpiperazino group was calculated to be 8.6 using Jaguar Software. The resulted low energy structures show that the ligand was stabilized inside the binding pocket mainly in a similar position as described previously.[20] Upon binding to FcyB, the protonated tertiary nitrogen forms salt bridge with Glu397. Additionally, two other hydrogen bonds are formed between N3H and Asn163 amide carbonyl group, while $\text{C}2=\text{O}$ interacts with NH_2 of Asn354 side chain. Finally, an extra H-bond seems to be possible between N1H and Ser261. Trp159 shows π - π stacking interactions with 3-deaza aromatic ring. (**Figure 4A, C**). In the case of compound **11e**, the bulky 2-[(2,5-dimethoxy)phenyl] group forms the π - π stacking interactions with Trp159 while two hydrogen bonds are formed one between Glu397 and the N4H and the second between Ser85 side chain and the methoxy group of the 2-substituent (**Figure 4B, D**).

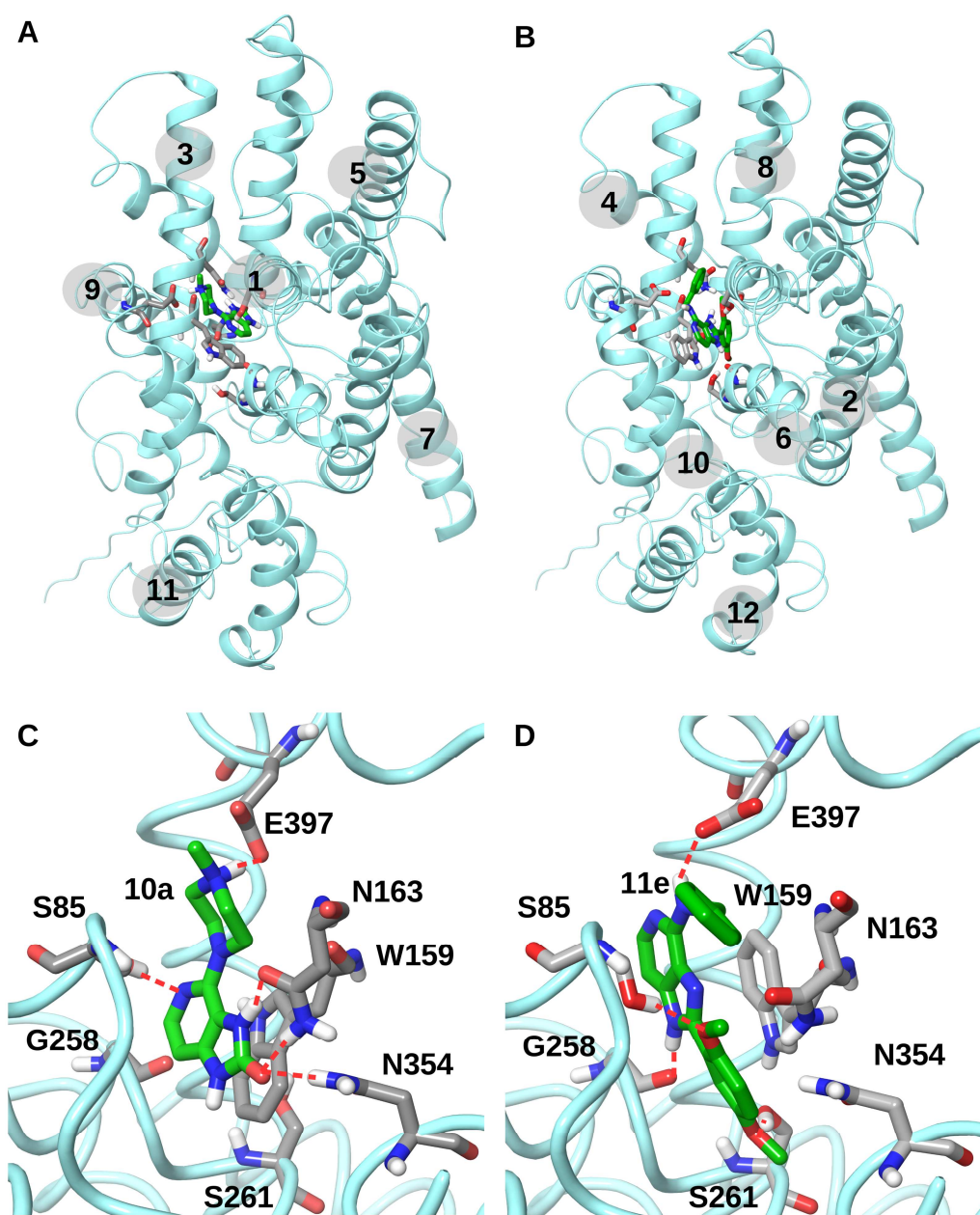


Figure 4: Low energy binding mode of compounds **10a** (A) and **11e** (B) in complex with FcyB as resulted by docking calculations. C and D detailed presentation of the interactions in the binding cavity for **10a** and **11e** (in green) correspondingly. Hydrogen bonds are depicted with red dashed lines.

2.6 Molecular Dynamics of FcyB in complex with analogue 10a. To further address aspects of molecular recognition and dynamic behavior, a study of the protein-ligand interactions has been undertaken for FcyB in complex with compound **10a** using molecular dynamics. Initially the ligand was positioned in a location similar to the corresponding to the hydantoin derivative in the parent Mhp1 crystal structure used for template (pdb: 4d1d) and a 90 ns simulation was carried out. The MD trajectory shows that the protein remains relatively stable as depicted by the small variations of the overall Ca RMSD from the 30th ns till the end of the simulation (**Figure S1A**). The residue RMS fluctuations ranged from 0.8 Å for rigid secondary structural elements to 6 Å for mobile loops (**Figure S1B**). The most important conformational change of the protein seems to be the reorientation of TMH10, taking place mainly till

the 30th ns. This reorientation of TMH10 displaces the Glu401 of ~ 4 Å and all residues 386-400 in the loop between TMH9-TMH10 (**Figure 5A**).

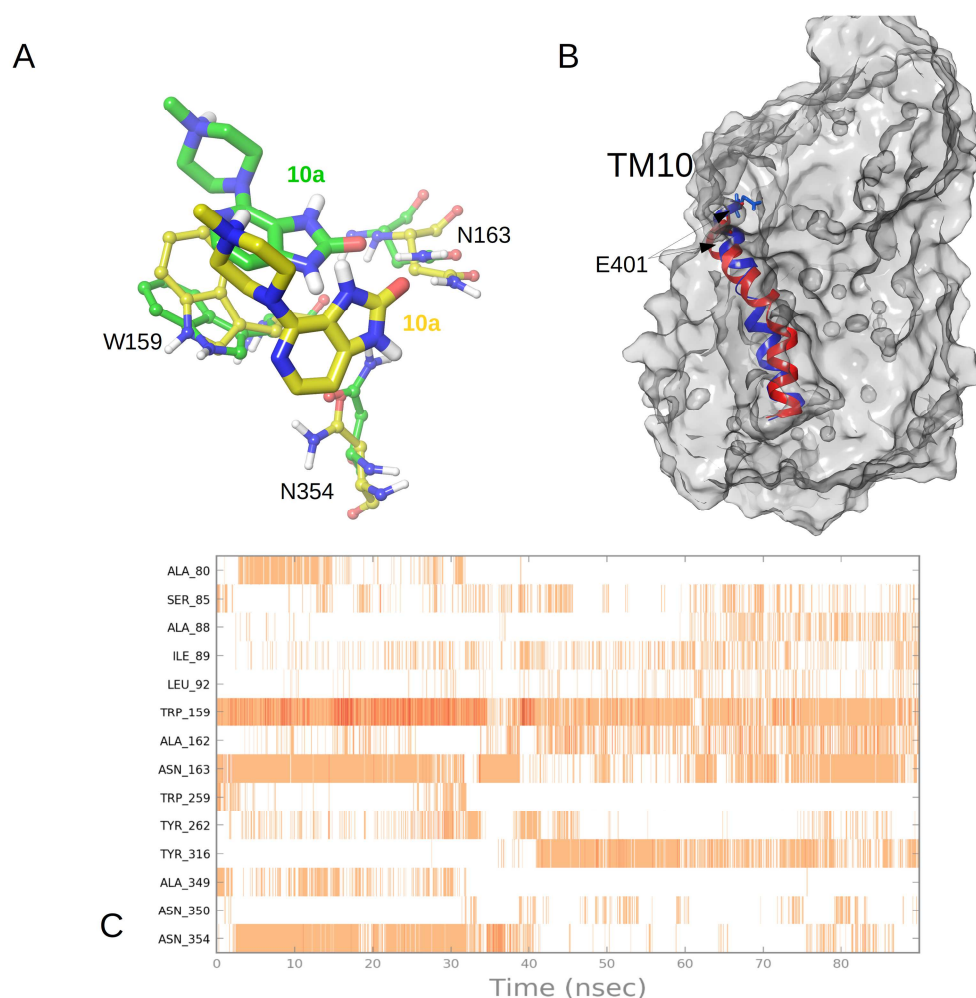


Figure 5. Molecular Dynamic Analysis of Fcyb in complex with compound 10a. A. Superposition of the binding site of FcyB in complex with compound **10a**: Initial pose of MD simulation (t=0 ns, yellow) and final pose of MD simulation (t=90ns, green). B. Superposition of starting (cyan) and ending (red) position of TMH10 after 90ns of simulation time. C. Timeline representation of interactions of compound **10a** during the MD simulation. The panel shows which residue interacts with the ligand in each trajectory frame. Dark shades of orange indicate more than one specific contact.

The ligand **10a** remains in the binding cavity although during of the simulation is displaced by ~ 3 Å towards the protein surface (**Figure 5B**). During the initial part till the 40th ns the ligand forms HB mainly with Asn163 and Asn354 while it displays weaker interactions with Tyr262 and Ser85. It is then relocated losing contact with Asn354 and Tyr262. During the whole simulation the ligand forms a pi-pi interaction with Trp159 and till the end it remains between Asn163, Trp159 and Ile89 (**Figure 5C**). It is interesting that Trp259 remains parallel to the ligand however interactions are rare specifically between 0- 30 ns then the ligand moves away and there is no interaction after. The charged quaternary piperazine nitrogen initially forms contacts with Glu397 and Glu401 (the later through a water molecule). However its displacement and the simultaneous shift of TMH10 reorients the residues' side chains

weakening and finally eliminating those interactions, leaving the piperazine moiety mainly surrounded by water molecules (data not shown).

3. DISCUSSION

The *A. nidulans* purine/H⁺ symporters FcyB and AzgA belong to evolutionary and structurally distinct transporter families (NCS1 and NAT/NCS2, respectively), but display very similar, high-affinity, binding for adenine, hypoxanthine and guanine. However, their substrate binding sites should be significantly different, as revealed by their binding affinities for cytosine (recognized only by FcyB) or other, non-physiological substrates, such as the drugs 5-fluorocytosine (FcyB) or 8-azaguanine (AzgA). We have previously reported a model of FcyB based on the first crystal structure of the bacterial homologue Mhp1.[7] In the same report we identified, via substrate docking approaches and rational mutational analysis, residues essential for the function and specificity that seem to define the substrate-binding site of FcyB. Furthermore, we have subsequently shown that 3-deazaadenine derivatives bearing substitutions on positions 1 and 4, inhibit the transport of physiological substrates.[20] Here we present a refined model of FcyB structure built upon homology threading to the updated, outward-facing, crystal structure of Mhp1. This new FcyB model shows that the side chains of all five residues that have been shown previously to be critical for transport activity, namely Ser85 (TMH1), Trp159, Asn163 (TMH3), Trp259 (TMH6) and Asn354 (TMH8), protrude to the substrate-binding cavity of the transporter. Using the improved FcyB model, we evaluated, as inhibitors of FcyB and two other *A. nidulans* purine transporters, novel 3-deazaadenine analogues, which were rationally designed based on our previous relative experience.

The synthesized compounds tested in this work expand the study on FcyB-ligand interactions. They firstly show that substitution at both positions 2 and 4 can antagonize adenine uptake, with similar inhibitory activities to some of the previously tested 3-deazaadenine derivatives. The introduction of a carbonyl group in position 3 of 3-deazaadenine enhances dramatically binding to FcyB, since compounds **10a** and **11a** exhibit 10- and 5-fold higher inhibitory activity when compared to the parent molecules **4** and **3**. This suggests that the carbonyl group participates actively in protein-ligand interactions, confirming the model proposed in **Figure 4A, C**, which shows that the major interaction of FcyB with the purine ring occurs via H-bonding with residues Asn163 and Asn354. A very similar pattern has been observed in the crystal structure of hydantoin bound to Mhp1 forming H-bonds with the corresponding Glu121 and Asn318.[13] This is also in agreement with the observation that conversion of carbonyl oxygen to sulfur in the thiourea analogues **10b** and **11b** decreases the inhibitory activity, as the corresponding interactions formed by sulfur are expected to be weaker. The carbonyl substitution is also advantageous when comparing derivative **10a** to **2**, both bearing a 4-methylpiperazine substituent at position 4. This trend is inversed in the case of the **11a** and **1** pair bearing a benzylamino substitution at the same position. In this case the carbonyl substitution is detrimental, decreasing the inhibitory activity ten-fold. According to the models derived by docking calculations this is probably due to the fact that in **1** the contribution for the protein-ligand interaction stems from the bidentate H-bonding formation between the NH at position 4 and N3 with the Asn163 amide, while this not the case in **11a** where interactions involving C2=O and N3H with Asn163 are apparently weaker. Other substitutions than the OH at position 2 can still produce interesting activities with most surprising the 2,5-dimethoxyphenyl substitution that proved to be the most active derivative of the **11a-f** series. Compound **11e** seems to be

displaced in the outer part of the binding cavity in such orientation that can form appropriate hydrophobic interactions via the 2,5-dimethoxyphenyl moiety and H-bonding between all different nitrogen atoms with surrounding residue side chains (**Figure 4B, D**) resulting to an increased activity.

A critical point of our present work, but also of our previous relative work, concerns the specificity of the compounds tested against FcyB. All compounds exhibiting important inhibitory activity display significantly increased specificity for FcyB, compared to AzgA (**Figure 3**). Although AzgA and FcyB fold in completely different structures, they both transport adenine, hypoxanthine or guanine. The major interaction in the AzgA cavity is between the substrate and two carboxylates from Glu339 and Asp394.[6] In this case, interactions are completely different and specificity is driven by a complex multiplicity of interactions. It is noticeable that the parent compounds **4** and **3** do not show any significant-inhibitory activity to either AzgA or FcyB, however the urea compounds **10a** and **11a** do exhibit significant binding specificity. Interestingly substitution at position 2 by a 4-NO₂-phenyl moiety abolishes specificity, compound **10c** being one of the most actives against AzgA along with the 2-(2-OH-phenyl)-substituted **11d**. Those compounds form the basis for further development of new optimized structures targeting AzgA. Although from the point of view of basic science, the distinct FcyB selectivity over AzgA is important as it shows that highly specific transporter drugs can indeed be rationally designed, for the purpose of a therapeutic antifungal activity, the discovery or design of dual inhibitors acting on several fungal-specific transporters might prove even more valuable. In this direction, analogues **10c** or **11d** (see Figure 3) seem as promising starting compounds to inhibit both FcyB and AzgA fungal nucleobase transporters.

Solute transport is associated with major changes in the structure of transporters. High-resolution structures of the Mhp1 transporter suggest that during the transport cycle the transition from the outward-open to occluded and then to the inward-open conformation, a semi-rigid body rotation occurs between hash and bundle motifs while TMH10 bends as an extracellular gate to close the binding cavity, accompanied by a bending of TMH5 operating as an intracellular gate. Upon binding of the substrate TMH10 twists over the substrate closing the extracellular gate and occluding it in the binding cavity. The importance of the TMH10 reorientation is also shown in the well-studied 5HIR transporter LeuT, where the extracellular gate is closed through the formation of a salt-bridge between Arg30 (TMH1b) and Asp404 (TMH10) along with other interactions between the two helices. The importance of TMH10 in transport has also been shown in the case of FurD, where site-specific mutations in TMH10 result to enlarged specificity.[10] In the complex of FcyB with the most active compound of these series, namely **10a**, MD simulations suggested that the ligand is stabilized in a position different than the corresponding one in the case of hydantoin-Mhp1 complex. After 90 ns of simulation the ligand is displaced ~3 Å towards the outer part of the cavity. In this position, **10a** is stabilized by forming HBs with Asn163 and Ser85 as well as pi-pi stacking with Trp159, while the “rest” of the analogue is mainly solvated by a sphere of water molecules. Although the starting structure was constructed upon the outward-facing conformation of Mhp1, the new position of **10a** in the cavity tilts the TMH10 further away. This dynamic behavior confirms that this compound acts as a competitive inhibitor of transport. In that sense scaffolds based on **10a** are interesting not only as chemical biology tools for the study of similar purine transporters, but also can be considered for further development of specific transporter-targeted antifungal drugs.

In conclusion, we have identified seven new compounds with relatively high affinity for the FcyB binding site. Importantly three of these compounds can also efficiently inhibit AzgA, a structurally and evolutionary distinct, but functionally similar, fungal purine transporter. None of the new compounds had any effect on the transport activity of the uric acid-xanthine transporter UapA, albeit this being a structural homologue of AzgA. Besides the apparent importance for understanding how nucleobase transporter specificity is determined at the molecular level, our work might constitute a critical step in the design of novel purine-related antifungals.

4. METHODS

4.1 Chemistry. Melting points were determined on a Büchi apparatus and are uncorrected. ^1H NMR spectra and 2D spectra were recorded on a Bruker Avance III 600 or a Bruker Avance DRX 400 instrument, whereas ^{13}C NMR spectra were recorded on a Bruker Avance III 600 or a Bruker AC 200 spectrometer in deuterated solvents and were referenced to TMS (δ scale). The signals of ^1H and ^{13}C spectra were unambiguously assigned by using 2D NMR techniques: $^1\text{H}^1\text{H}$ COSY, NOESY, HMQC, and HMBC. Mass spectra were recorded with a LTQ Orbitrap Discovery instrument, possessing an Ionmax ionization source. Flash chromatography was performed on Merck silica gel 60 (0.040–0.063 mm). Analytical thin layer chromatography (TLC) was carried out on precoated (0.25 mm) Merck silica gel F-254 plates.

4.1.1 Synthesis and characterization of compounds 10a-f, 11a-f, 12a-f

4.1.1.1. 4-(4-Methylpiperazin-1-yl)-1,3-dihydroimidazo[4,5-c]pyridin-2-one (10a)

A solution of the nitro derivative **8** (240 mg, 1.0 mmol) in absolute ethanol (60 mL) was hydrogenated in the presence of 10% Pd/C (90 mg) at 35 psi for 4h. The solution was filtered through a celite pad to remove the catalyst and the filtrate was evaporated to dryness. To a solution of the resulting diamine (210 mg, 1.0 mmol) in tetrahydrofuran (10 mL), 1,1'-carbonyldiimidazole was added (325 mg, 2.0 mmol) and the mixture was heated at reflux for 24h. Then, the organic solvent was evaporated under vacuo and the residue was purified using silica gel column chromatography (dichloromethane/methanol: 8/2). White solid, 230 mg (98%), m.p. $>250^\circ\text{C}$ (methanol/ether). ^1H NMR (400 MHz, DMSO- d_6) δ 10.97 (s, 1H, NH), 10.75 (s, 1H, NH), 7.75 (d, $J = 5.3$ Hz, 1H, H-6), 6.60 (d, $J = 5.3$ Hz, 1H, H-7), 3.20 (m, 4H, piperazine H-2,6), 2.45 (m, 4H, piperazine H-3,5), 2.21 (s, 3H, NCH₃). ^{13}C NMR (151 MHz, DMSO- d_6) δ 154.70 (C-2), 145.26 (C-4), 139.46 (C-6), 136.49 (C-7a), 114.93 (C-3a), 99.55 (C-7), 54.60 (piperazine C-3,5), 47.35 piperazine (C-2,6), 45.84 (NCH₃). HRMS-ESI(-) (C₁₁H₁₄N₅O) [M-H]⁻ m/z calcd 232.1193, found 232.1198.

4.1.1.2. 4-(4-Methylpiperazin-1-yl)-1,3-dihydroimidazo[4,5-c]pyridine-2-thione (10b)

This compound was synthesized using a procedure analogous to that of **10a**, using 1,1'-thiocarbonyldiimidazole. The residue was purified using silica gel column chromatography (dichloromethane/methanol: 9/1). Beige solid, yield 68%, m.p. $>250^\circ\text{C}$ (methanol/ether). ^1H NMR (400 MHz, DMSO- d_6) δ 13.25-12.45 (brs, 2H, NH), 7.87 (d, $J = 5.4$ Hz, 1H, H-6), 6.75 (d, $J = 5.4$ Hz, 1H, H-7), 3.33 (m, 4H, piperazine H-2,6), 2.50 (m, 4H, piperazine H-3,5), 2.25 (s, 3H, NCH₃). ^{13}C NMR (151 MHz, DMSO- d_6) δ 168.21 (C-2), 145.87 (C-4), 140.60 (C-6), 139.01 (C-7a), 118.19 (C-3a), 99.29 (C-7), 54.49 (piperazine C-3,5), 47.36 (piperazine C-2,6), 45.75 (NCH₃). HRMS-ESI(-) (C₁₁H₁₄N₅S) [M-H]⁻ m/z calcd 248.0964, found 248.0969.

4.1.1.3. 4-(4-Methylpiperazin-1-yl)-2-(4-nitrophenyl)-1H-imidazo[4,5-c]pyridine (10c)

To a solution of **8** (210 mg, 1.0 mmol) in toluene (10 mL), was added montmorillonite K-10 (300 mg) followed by 4-nitrobenzaldehyde (166 mg, 1.1 mmol) and the mixture was heated at reflux for 24h. Then, the organic solvent was evaporated under vacuo and the residue was purified using silica gel column chromatography (dichloromethane/methanol: 9/1) to provide **10c** as a brown solid, 200mg (59%), m.p.>250°C (ethanol/ether). ¹H NMR (400 MHz, DMSO-*d*₆) δ 13.64-13.34 (brs, 1H, NH), 8.40 (d, *J* = 8.9 Hz, 2H, H-3',5'), 8.35 (d, *J* = 8.9 Hz, 2H, H-2',6'), 7.84 (d, *J* = 5.6 Hz, 1H, H-6), 6.91 (d, *J* = 5.6 Hz, 1H, H-7), 4.16 (m, 4H, piperazine H-2,6), 2.54 (m, 4H, piperazine H-3,5), 2.28 (s, 3H, NCH₃). ¹³C NMR (151 MHz, DMSO-*d*₆) δ 151.12 (C-4), 147.69 (C-4'), 145.91 (C-2), 141.26 (C-7a), 140.73 (C-6), 135.51 (C-1'), 128.87 (C-3a), 127.18 (C-2',6'), 124.34 (C-3',5'), 98.52 (C-7), 54.61 (piperazine C-3,5), 45.64 (piperazine C-2,6), 45.51 (NCH₃). HRMS-ESI(-) (C₁₇H₁₇N₆O₂) [M-H]⁻ m/z calcd 337.1408, found 337.1412.

4.1.1.4. 2-(2-Hydroxyphenyl)-4-(4-methylpiperazin-1-yl)-1*H*-imidazo[4,5-*c*]pyridine (**10d**)

This compound was synthesized using a procedure analogous to that of **10c**. The residue was purified using silica gel column chromatography (dichloromethane/methanol: 9/1) and upon successive preparative thin layer chromatography (chloroform/methanol: 9/1), compound **10d** was isolated as a beige solid, yield 47%, m.p. 224-225°C (ether), together with a small amount of **13**. Data for **10d**: ¹H NMR (600 MHz, DMSO-*d*₆) δ 13.47 – 13.02 (brs, 1H, NH), 12.47 – 12.03 (brs, 1H, OH), 8.05 (d, *J* = 7.5 Hz, 1H, H-6'), 7.87 (d, *J* = 5.2 Hz, 1H, H-6), 7.37 (t, *J* = 7.5 Hz, 1H, H-4'), 7.02 (m, 2H, H-3',5'), 6.99 (d, *J* = 5.2 Hz, 1H, H-7), 4.00 (m, 4H, piperazine H-2,6), 2.57 (m, 4H, piperazine H-3,5), 2.30 (s, 3H, NCH₃). ¹³C NMR (151 MHz, DMSO-*d*₆) δ 157.16 (C-2'), 150.39 (C-4), 148.81 (C-2), 140.21 (C-6), 139.93 (C-7a), 131.54 (C-4'), 126.59 (C-6'), 126.10 (C-3a), 119.35 (C-5'), 116.99 (C-3'), 112.98 (C-1'), 99.14 (C-7), 54.64 (piperazine C-3,5), 46.02 (piperazine C-2,6), 45.86 (NCH₃). HRMS-ESI(-) (C₁₇H₁₈N₅O) [M-H]⁻ m/z calcd 308.1506, found 308.1510.

Data for 1-[(2-hydroxyphenyl)methyl]-2-(2-hydroxyphenyl)-4-(4-methylpiperazin-1-yl)-1*H*-imidazo[4,5-*c*]pyridine (**13**): beige solid, yield 4%, m.p. 165-166°C (methanol). ¹H NMR (600 MHz, DMSO-*d*₆) δ 10.54-10.10 (brs, 1H, OH), 10.05-9.65 (brs, 1H, OH), 7.76 (d, *J* = 5.7 Hz, 1H, H-6), 7.33 (d, *J* = 7.5 Hz, 2H, H-3',5') 7.01 (m, 2H, H-6',4''), 6.89 (m, 1H, H-4'), 6.76 (m, 1H, H-3''), 6.72 (d, *J* = 5.7 Hz, 1H, H-7), 6.58 (t, *J* = 7.4 Hz, 1H, H-5''), 6.36 (d, *J* = 7.4 Hz, 1H, H-6''), 5.23 (s, 2H, CH₂), 4.05 (m, 4H, piperazine H-2,6), 2.44 (m, 4H, piperazine H-3,5), 2.22 (s, 3H, NCH₃). ¹³C NMR (151 MHz, DMSO-*d*₆) δ 155.85 (C-2'), 154.58 (C-2''), 150.96 (C-4), 149.14 (C-2), 141.14 (C-7a), 139.56 (C-6), 131.35 (C-3'), 128.35 (C-4''), 127.44 (C-3a), 127.02 (C-6''), 126.80 (C-1'), 122.45 (C-1''), 119.13 (C-4'), 118.80 (C-5''), 117.11 (C-5'), 115.90 (C-6'), 114.88 (C-3''), 97.93 (C-7), 54.59 (piperazine C-3,5), 45.64 (NCH₃), 45.51 (piperazine C-2,6), 42.83 (CH₂). The ¹³C NMR chemical shifts for this compound were extracted from the corresponding HMBC spectrum. HRMS-ESI(+) (C₂₄H₂₆N₅O₂) [M+H]⁺ m/z calcd 416.2081, found 416.2080.

4.1.1.5. 2-(2,5-Dimethoxyphenyl)-4-(4-methylpiperazin-1-yl)-1*H*-imidazo[4,5-*c*]pyridine (**10e**)

This compound was synthesized using a procedure analogous to that of **10c**. The residue was purified using silica gel column chromatography (dichloromethane/methanol: 9/1) and the product was obtained as a yellow solid, yield 42%, m.p. 180-181°C (n-hexane). ¹H NMR (600 MHz, DMSO-*d*₆) δ 12.34-12.20 (brs, 1H, NH), 7.79 (d, *J* = 5.5 Hz, 1H, H-6), 7.76 (d, *J* = 3.2 Hz, 1H, H-6'), 7.15 (d, *J* =

9.0 Hz, 1H, H-3'), 7.05 (dd, $J = 9.0, 3.2$ Hz, 1H, H-4'), 6.97 (d, $J = 5.5$ Hz, 1H, H-7), 4.14 (m, 4H, piperazine H-2,6), 3.94 (s, 3H, 2'-OCH₃), 3.78 (s, 3H, 5'-OCH₃), 2.57 (m, 4H, piperazine H-3,5), 2.28 (s, 3H, NCH₃). ¹³C NMR (151 MHz, DMSO-*d*₆) δ 153.23 (C-5'), 151.06 (C-2'), 150.78 (C-4), 145.70 (C-2), 140.61 (C-7a), 139.48 (C-6), 127.80 (C-3a), 118.35 (C-1'), 116.27 (C-4'), 114.57 (C-6'), 113.36 (C-3'), 99.48 (C-7), 56.18 (2'-OCH₃), 55.62 (5'-OCH₃), 54.53 (piperazine C-3,5), 45.52 (NCH₃-piperazine C-2,6). HRMS-ESI(-) (C₁₉H₂₂N₅O₂) [M-H]⁻ m/z calcd 352.1768, found 352.1770.

4.1.1.6. 4-(4-Methylpiperazin-1-yl)-2-(pyridin-4-yl)-1H-imidazo[4,5-*c*]pyridine (10f)

This compound was synthesized using a procedure analogous to that of **10c**. The residue was purified using silica gel column chromatography (dichloromethane/methanol: 9/2) and upon successive preparative thin layer chromatography (chloroform/methanol: 9/2) compound **10f** was isolated as yellow oil (yield 28%), together with a small amount of **14**. Data for **10f**: ¹H NMR (600 MHz, DMSO-*d*₆) δ 13.80-13.10 (brs, 1H, NH), 8.74 (d, $J = 5.7$ Hz, 2H, H-2',6'), 8.04 (d, $J = 5.7$ Hz, 2H, H-3',5'), 7.84 (d, $J = 5.6$ Hz, 1H, H-6), 6.90 (d, $J = 5.6$ Hz, 1H, H-7), 4.14 (m, 4H, piperazine H-2,6), 2.46 (m, 4H, piperazine H-3,5), 2.23 (s, 3H, NCH₃). ¹³C NMR (151 MHz, DMSO-*d*₆) δ 151.22 (C-4), 150.49 (C-2',6'), 145.66 (C-2), 141.09 (C-7a), 140.66 (C-6), 136.62 (C-4'), 128.61 (C-3a), 120.13 (C-3',5'), 98.50 (C-7), 54.78 (piperazine C-3,5), 45.90 (NCH₃), 45.69 (piperazine C-2,6). HRMS-ESI(-) (C₁₆H₁₇N₆) [M-H]⁻ m/z calcd 293.1509, found 293.1512

Data for 4-(4-methylpiperazin-1-yl)-1-[(pyridin-4-yl)methyl]-2-(4-pyridyl)-1H-imidazo[4,5-*c*]pyridine (**14**): Yellow oil, Yield 4%. ¹H NMR (600 MHz, DMSO-*d*₆) δ 8.70 (d, $J = 6.0$ Hz, 1H, H-2',6'), 8.47 (d, $J = 5.8$ Hz, 1H, H-2'',6''), 7.86 (d, $J = 5.7$ Hz, 1H, H-6), 7.66 (d, $J = 6.0$ Hz, 1H, H-3',5'), 6.97 (d, $J = 5.8$ Hz, 1H, H-3'',5''), 6.87 (d, $J = 5.7$ Hz, 1H, H-7), 5.66 (s, 2H, CH₂), 4.13 (m, 4H, piperazine H-2,6), 2.45 (m, 4H, piperazine H-3,5), 2.22 (s, 3H, NCH₃). ¹³C NMR (151 MHz, DMSO-*d*₆) δ 151.32 (C-4), 150.29 (C-2',6'), 150.10 (C-2'',6''), 147.17 (C-2), 145.36 (C-4''), 142.59 (C-7a), 141.08 (C-6), 136.74 (C-4'), 127.29 (C-3a), 122.96 (C-3',5'), 121.16 (C-3'',5''), 97.50 (C-7), 54.80 (piperazine C-3,5), 46.75 (CH₂), 45.94 (NCH₃), 45.66 (piperazine C-2,6). HRMS-ESI(+) (C₂₂H₂₄N₇) [M+H]⁺ m/z calcd 386.2088, found 386.2089.

4.1.1.7. 4-Benzylamino-1,3-dihydroimidazo[4,5-*c*]pyridin-2-one (11a) and 7-amino-3-benzyl-3H-imidazo[4,5-*b*]pyridin-2-one (12a)

These compounds were synthesized using a procedure analogous to that of **10a**. The residue was purified using silica gel column chromatography (ethyl acetate/methanol: 9/1) and each isomer was isolated using preparative thin layer chromatography (dichloromethane/methanol 95:5).

Data for **11a**: Yield 15%, white solid, m.p. 197-198°C (ether), ¹H NMR (600 MHz, Acetone-*d*₆) δ 9.90-9.82 (brs, 1H, imidazole NH), 9.48-9.40 (brs, 1H, imidazole NH), 7.73 (d, $J = 5.4$ Hz, 1H, H-6), 7.40 (d, $J = 7.6$ Hz, 2H, benzylamine H-2,6), 7.31 (t, $J = 7.3$ Hz, 2H, benzylamine H-3,5), 7.23 (t, $J = 7.3$ Hz, 1H, benzylamine H-4), 6.47 (d, $J = 5.4$ Hz, 1H, H-7), 5.71 (s, 1H, benzylamine NH), 4.71 (d, $J = 5.5$ Hz, 2H, benzylamine CH₂). ¹³C NMR (151 MHz, Acetone-*d*₆) δ 155.12 (C-2), 144.16 (C-4), 141.62 (benzylamine C-1), 141.20 (C-6), 136.06 (C-7a), 129.18 (benzylamine C-3,5), 128.57 (benzylamine C-2,6), 127.62 (benzylamine C-4), 112.10 (C-3a), 97.72 (C-7), 45.55 (benzylamine CH₂). HRMS-ESI(-) (C₁₃H₁₁N₄O) [M-H]⁻ m/z calcd 239.0938, found 239.0945).

Data for **12a**: Yield 35%, brown solid m.p. 256-257°C (ether), ¹H NMR (600 MHz, DMSO-*d*₆) δ 10.34-10.28 (brs, 1H, NH), 7.56 (d, *J* = 5.7 Hz, 1H, H-5), 7.29 (m, 4H, benzyl H-2,3,5,6), 7.23 (m, 1H, benzyl H-4), 6.33 (d, *J* = 5.7 Hz, 1H, H-6), 5.77 (s, 2H, NH₂), 4.93 (s, 2H, benzyl CH₂). ¹³C NMR (151 MHz, DMSO-*d*₆) δ 152.68 (C-2), 143.90 (C-3a), 141.31 (C-5), 137.77 (benzyl C-1), 137.35 (C-7), 128.37 (benzyl C-3,5), 127.39 (benzyl C-2,6), 127.13 (benzyl C-4), 107.33 (C-7a), 104.95 (C-6), 42.12 (benzyl CH₂). HRMS-ESI (+) (C₁₃H₁₃N₄O) [M+H]⁺ *m/z* calcd 241.1084, found 241.1086).

4.1.1.8. 4-Benzylamino-1,3-dihydroimidazo[4,5-*c*]pyridine-2-thione (11b) and 7-amino-3-benzyl-3*H*-imidazo[4,5-*b*]pyridine-2-thione (12b)

These compounds were synthesized using a procedure analogous to that of **10a**. The residue was purified using silica gel column chromatography (cyclohexane/ethyl acetate: 1/2) and each isomer was isolated using preparative thin layer chromatography (dichloromethane/methanol 95:5).

Data for **11b**: Yield 15%, brown solid m.p. 250-251°C (ether), ¹H NMR (600 MHz, Acetone-*d*₆) δ 11.54-11.40 (brs, 1H, imidazole NH), 11.37-11.20 (brs, 1H, imidazole NH), 7.82 (d, *J* = 5.6 Hz, 1H, H-6), 7.43 (d, *J* = 7.6 Hz, 2H, benzylamine H-2,6), 7.32 (t, *J* = 7.6 Hz, 2H, benzylamine H-3,5), 7.25 (t, *J* = 7.4 Hz, 1H, benzylamine H-4), 6.61 (d, *J* = 5.6 Hz, 1H, H-7), 6.13-6.10 (brs, 1H, benzylamine NH), 4.75 (d, *J* = 5.2 Hz, 2H, benzylamine CH₂). ¹³C NMR (151 MHz, Acetone-*d*₆) δ 169.64 (C-2), 144.37 (C-4), 142.52 (C-6), 141.00 (benzylamine C-1), 138.78 (C-7a), 129.24 (benzylamine C-3,5), 128.62 (benzylamine C-2,6), 127.77 (benzylamine C-4), 115.96 (C-3a), 97.38 (C-7), 45.55 (benzylamine CH₂). HRMS-ESI(+) (C₁₃H₁₃N₄S) [M+H]⁺ *m/z* calcd 257.0855, found 257.0861)

Data for **12b**: Yield 30%, white solid m.p. 262-263°C (ether), ¹H NMR (600 MHz, DMSO-*d*₆) δ 13.07-11.68 (brs, 1H, NH), 7.74 (d, *J* = 5.5 Hz, 1H, H-5), 7.37 (d, *J* = 7.3 Hz, 2H, benzyl H-2,6), 7.29 (t, *J* = 7.4 Hz, 2H, benzyl H-3,5), 7.23 (t, *J* = 7.1 Hz, 1H, benzyl H-4), 6.43 (d, *J* = 5.5 Hz, 1H, H-6), 6.17 (s, 2H, NH₂), 5.37 (s, 2H, benzyl CH₂). ¹³C NMR (151 MHz, DMSO-*d*₆) δ 166.36 (C-2), 145.87 (C-3a), 143.74 (C-5), 138.55 (C-7), 136.85 (benzyl C-1), 128.25 (benzyl C-3,5), 127.74 (benzyl C-2,6), 127.23 (benzyl C-4), 110.89 (C-7a), 104.73 (C-6), 44.92 (benzyl CH₂). HRMS-ESI(+) (C₁₃H₁₃N₄S) [M+H]⁺ *m/z* calcd 257.0855, found 257.0848).

4.1.1.9. *N*-Benzyl-2-(4-nitrophenyl)-1*H*-imidazo[4,5-*c*]pyridin-4-amine (11c) and 3-benzyl-2-(4-nitrophenyl)-3*H*-imidazo[4,5-*b*]pyridin-7-amine (12c)

These compounds were synthesized using a procedure analogous to that of **10c**. The residue was purified using silica gel column chromatography (ethyl acetate) and each isomer was isolated using preparative thin layer chromatography (ethyl acetate).

Data for **11c**: Yield 25%, yellow solid m.p.: 255-256°C (ether), ¹H NMR (600 MHz, Acetone-*d*₆) δ 12.23-11.28 (brs, 1H, imidazole NH), 8.40 (d, *J* = 8.9 Hz, 2H, nitrophenyl H-3,5), 8.36 (d, *J* = 8.9 Hz, 2H, nitrophenyl H-2,6), 7.80 (d, *J* = 5.8 Hz, 1H, H-6), 7.46 (d, *J* = 7.5 Hz, 2H, benzylamine H-2,6), 7.30 (t, *J* = 7.6 Hz, 2H, benzylamine H-3,5), 7.21 (t, *J* = 7.4 Hz, 1H, benzylamine H-4), 6.81 (d, *J* = 5.8 Hz, 1H, H-7), 6.78-6.71 (brs, 1H, benzylamine NH), 4.90 (s, 2H, benzylamine CH₂). ¹³C NMR (151 MHz, Acetone-*d*₆) δ 152.30 (C-4), 149.07 (nitrophenyl C-1), 148.14 (nitrophenyl C-4), 142.21 (C-3a), 141.98 (C-6), 137.01 (C-2), 129.09 (benzylamine C-3,5), 128.42 (benzylamine C-2,6), 127.96 (nitrophenyl C-3,5), 127.47 (benzylamine C-4), 125.02 (nitrophenyl C-2,6), 98.62 (C-7), 45.00 (benzylamine CH₂). HRMS-ESI(-) (C₁₉H₁₄N₅O₂) [M-H]⁻ *m/z* calcd 344.1153, found 344.1141).

Data for **12c**: Yield 35%, yellow solid m.p.: 198-199°C (methanol), ¹H NMR (600 MHz, DMSO-*d*₆) δ 8.32 (d, *J* = 8.8 Hz, 2H, nitrophenyl H-3,5), 8.01 (d, *J* = 8.8 Hz,

2H, nitrophenyl H-2,6), 7.90 (d, $J = 5.5$ Hz, 1H, H-5), 7.24 (t, $J = 7.3$ Hz, 2H, benzyl H-3,5), 7.19 (t, $J = 7.2$ Hz, 1H, benzyl H-4), 6.98 (d, $J = 7.3$ Hz, 2H, benzyl H-2,6), 6.61 (s, 2H, NH₂), 6.46 (d, $J = 5.5$ Hz, 1H, H-6), 5.62 (s, 2H, benzyl CH₂). ¹³C NMR (151 MHz, DMSO-*d*₆) δ 149.19 (C-2), 147.64 (nitrophenyl C-4), 147.17 (C-3a), 147.00 (C-7), 145.74 (C-5), 137.18 (benzyl C-1), 136.58 (nitrophenyl C-1), 129.70 (nitrophenyl C-2,6), 128.64 (benzyl C-3,5), 127.35 (benzyl C-4), 126.29 (benzyl C-2,6), 123.80 (nitrophenyl C-3,5), 122.95 (C-7a), 102.84 (C-6), 45.94 (benzyl CH₂). HRMS-ESI(+) (C₁₉H₁₆N₅O₂) [M+H]⁺ m/z calcd 346.1299, found 346.1288).

4.1.1.10. *N*-Benzyl-2-(2-hydroxyphenyl)-1*H*-imidazo[4,5-*c*]pyridin-4-amine (11d) and 3-benzyl-2-(2-hydroxyphenyl)-3*H*-imidazo[4,5-*b*]pyridin-7-amine (12d)

These compounds were synthesized using a procedure analogous to that of **10c**. The residue was purified using silica gel column chromatography (dichloromethane/methanol: 9/1) to provide compounds **11d** and **12d**.

Data for **11d**: Yield 15%, brown solid m.p.: 118-119°C (ether/n-pentane), ¹H NMR (600 MHz, Acetone-*d*₆) δ 12.54-12.36 (brs, 1H, imidazole NH), 12.32-12.14 (brs, 1H, OH), 7.94 (dd, $J = 7.8, 1.3$ Hz, 1H, hydroxyphenyl H-3), 7.83 (d, $J = 5.6$ Hz, 1H, H-6), 7.45 (d, $J = 7.5$ Hz, 2H, benzylamine H-3,5), 7.35 (td, $J = 7.8, 1.3$ Hz, 1H, hydroxyphenyl H-5), 7.29 (t, $J = 7.6$ Hz, 2H, benzylamine 2,6), 7.20 (t, $J = 7.4$ Hz, 1H, benzylamine H-4), 7.17-7.11 (brs, 1H, benzylamine NH), 7.01 (dd, $J = 7.8, 0.9$ Hz, 1H, hydroxyphenyl H-6), 6.96 (td, $J = 7.8, 0.9$ Hz, 1H, hydroxyphenyl H-4), 6.79 (d, $J = 5.6$ Hz, 1H, H-7), 4.88 (d, $J = 5.2$ Hz, 2H, benzylamine CH₂). ¹³C NMR (151 MHz, Acetone-*d*₆) δ 159.26 (C-2), 151.50 (C-4), 150.60 (hydroxyphenyl C-1), 142.37 (C-6), 142.15 (benzylamine C-1), 138.56 (C-7a), 132.23 (hydroxyphenyl C-5), 129.03 (benzylamine C-2,6), 128.40 (benzylamine C-3,5), 127.37 (benzylamine C-4), 126.38 (hydroxyphenyl C-3), 119.88 (hydroxyphenyl C-4), 118.28 (hydroxyphenyl C-6), 113.56 (hydroxyphenyl C-2), 97.97 (C-7), 44.83 (benzylamine CH₂). HRMS-ESI(+) (C₁₉H₁₇N₄O) [M+H]⁺ m/z calcd 317.1397, found 317.1407.

Data for **12d**: Yield 35%, white solid m.p.: 253-254°C (ether), ¹H NMR (600 MHz, DMSO-*d*₆) δ 11.43 (s, 1H, OH), 7.85 (d, $J = 5.5$ Hz, 1H, H-5), 7.41 (dd, $J = 7.7, 1.4$ Hz, 1H, hydroxyphenyl H-6), 7.32 (td, $J = 7.7, 1.4$ Hz, 1H, hydroxyphenyl H-4), 7.22 (t, $J = 7.3$ Hz, 2H, benzyl H-3,5), 7.18 (t, $J = 7.2$ Hz, 1H, benzyl H-4), 7.02 (dd, $J = 7.7, 0.8$ Hz, 1H, hydroxyphenyl H-3), 6.97 (d, $J = 7.3$ Hz, 2H, benzyl H-2,6), 6.84 (td, $J = 7.7, 0.8$ Hz, 1H, hydroxyphenyl H-5), 6.54 (s, 2H, NH₂), 6.43 (d, $J = 5.5$ Hz, 1H, H-6), 5.54 (s, 2H, benzyl CH₂). ¹³C NMR (151 MHz, DMSO-*d*₆) δ 156.61 (hydroxyphenyl C-2), 148.26 (C-2), 147.99 (C-7), 146.25 (C-3a), 144.93 (C-5), 137.36 (benzyl C-1), 131.15 (hydroxyphenyl C-4), 129.41 (hydroxyphenyl C-6), 128.48 (benzyl C-3,5), 127.18 (benzyl C-4), 126.40 (benzyl C-2,6), 121.32 (C-7a), 118.88 (hydroxyphenyl C-5), 116.64 (hydroxyphenyl C-3), 115.72 (hydroxyphenyl C-1), 102.79 (C-6), 46.06 (benzyl CH₂). HRMS-ESI(+) (C₁₉H₁₇N₄O) [M+H]⁺ m/z calcd 317.1397, found 317.1392.

4.1.1.11. *N*-Benzyl-2-(2,5-dimethoxyphenyl)-1*H*-imidazo[4,5-*c*]pyridin-4-amine (11e) and 3-benzyl-2-(2,5-dimethoxyphenyl)-3*H*-imidazo[4,5-*b*]pyridin-7-amine (12e)

These compounds were synthesized using a procedure analogous to that of **10c**. The residue was purified using silica gel column chromatography (dichloromethane/methanol: 19/1) to provide compounds **11e** and **12e**.

Data for **11e**: Yield 20%, brown solid m.p.: 190-191°C (ether/n-pentane), ¹H NMR (600 MHz, Acetone-*d*₆) δ 11.82-11.76 (brs, 1H, imidazole NH), 8.02 (d, $J = 3.1$ Hz, 1H, dimethoxyphenyl H-6), 7.74 (d, $J = 5.5$ Hz, 1H, H-6), 7.45 (d, $J = 7.5$ Hz, 2H, benzylamine H-2,6), 7.30 (t, $J = 7.5$ Hz, 2H, benzylamine H-3,5), 7.20 (t, $J = 7.3$ Hz,

1H, benzylamine H-4), 7.15 (d, $J = 9.0$ Hz, 1H, dimethoxyphenyl H-3), 7.01 (dd, $J = 9.0, 3.1$ Hz, 1H, dimethoxyphenyl H-4), 6.75 (d, $J = 5.5$ Hz, 1H, H-7), 6.53-6.49 (brs, 1H, benzylamine NH), 4.88 (d, $J = 5.8$ Hz, 2H, benzylamine CH₂), 4.00 (s, 3H, dimethoxyphenyl CH₃O-5), 3.81 (s, 3H, dimethoxyphenyl CH₃O-2). ¹³C NMR (151 MHz, Acetone-*d*₆) δ 154.88 (dimethoxyphenyl C-2), 152.16 (dimethoxyphenyl C-5), 152.09 (C-4), 148.02 (C-2), 142.33 (benzylamine C-1), 141.14 (C-6), 139.30 (C-7a), 129.05 (benzylamine C-3,5), 128.42 (benzylamine C-2,6), 128.09 (C-3a), 127.37 (benzylamine C-4), 119.61 (dimethoxyphenyl C-1), 117.45 (dimethoxyphenyl C-4), 114.76 (dimethoxyphenyl C-6), 113.94 (dimethoxyphenyl C-3), 98.72 (C-7), 56.57 (dimethoxyphenyl CH₃O-5), 56.06 (dimethoxyphenyl CH₃O-2), 44.97 (benzylamine CH₂). HRMS-ESI(-) (C₂₁H₁₉N₄O₂) [M-H]⁻ m/z calcd 359.1514, found 359.1498.

Data for **12e**: Yield 45%, orange solid m.p.: 90-91°C (ether/n-pentane), ¹H NMR (600 MHz, DMSO-*d*₆) δ 7.83 (d, $J = 5.5$ Hz, 1H, H-5), 7.16 (m, 3H, dimethoxyphenyl H-4, benzyl H-3,5), 7.07 (m, 2H, dimethoxyphenyl H-3, benzyl H-4), 6.88 (d, $J = 6.9$ Hz, 2H, benzyl H-2,6), 6.85 (d, $J = 2.6$ Hz, 1H, dimethoxyphenyl H-6), 6.40 (d, $J = 5.5$ Hz, 1H, H-6), 6.36 (s, 2H, NH₂), 5.21 (s, 2H, benzyl CH₂), 3.66 (s, 3H, dimethoxyphenyl CH₃O-2), 3.62 (s, 3H, dimethoxyphenyl CH₃O-5). ¹³C NMR (151 MHz, DMSO-*d*₆) δ 152.80 (dimethoxyphenyl C-2), 151.17 (dimethoxyphenyl C-5), 148.26 (C-2), 147.29 (dimethoxyphenyl C-1), 146.53 (C-3a), 144.59 (C-5), 137.44 (benzyl C-1), 128.14 (dimethoxyphenyl C-4), 126.99 (benzyl C-3,5), 126.79 (benzyl C-2,6), 122.68 (C-7), 120.27 (C-7a), 116.98 (dimethoxyphenyl C-6), 116.65 (dimethoxyphenyl C-3), 112.62 (benzyl C-4), 102.32 (C-6), 55.67 (dimethoxyphenyl CH₃O-2), 55.55 (dimethoxyphenyl CH₃O-5), 45.55 (benzyl CH₂). HRMS-ESI(+) (C₂₁H₂₁N₄O₂) [M+H]⁺ m/z calcd 361.1659, found 361.1655.

4.1.1.12. *N*-Benzyl-2-(pyridin-4-yl)-1*H*-imidazo[4,5-*c*]pyridin-4-amine (**11f**) and 3-benzyl-2-(pyridin-4-yl)imidazo[4,5-*b*]pyridin-7-amine (**12f**)

These compounds were synthesized using a procedure analogous to that of **6c**. The residue was purified using silica gel column chromatography (dichloromethane/methanol: 9/1) to provide compounds **11f** and **12f**.

Data for **11f**: Yield 25%, brown solid m.p.: 150-151°C (ether/n-pentane), ¹H NMR (600 MHz, Acetone-*d*₆) δ 12.78-11.75 (brs, 1H, NH imidazole), 8.71 (dd, $J = 4.5, 1.5$ Hz, 2H, pyridinyl H-3,5), 8.04 (dd, $J = 4.5, 1.5$ Hz, 2H, pyridinyl H-2,6), 7.81 (d, $J = 5.5$ Hz, 1H, H-6), 7.45 (d, $J = 7.7$ Hz, 2H, benzylamine H-2,6), 7.30 (t, $J = 7.6$ Hz, 2H, benzylamine H-3,5), 7.21 (t, $J = 7.4$ Hz, 1H, benzylamine H-4), 6.79 (d, $J = 5.5$ Hz, 1H, H-7), 6.70-6.65 (brs, 1H, benzylamine NH), 4.89 (d, $J = 4.9$ Hz, 2H, benzylamine CH₂). ¹³C NMR (151 MHz, Acetone-*d*₆) δ 152.40 (C-4), 151.45 (pyridinyl C-3,5), 147.78 (C-2), 142.31 (C-6), 142.03 (benzylamine C-1), 140.24 (C-7a), 138.00 (pyridinyl C-1), 129.12 (C-3a), 129.08 (benzylamine C-3,5), 128.41 (benzylamine C-2,6), 127.45 (benzylamine C-4), 120.90 (pyridinyl C-2,6), 98.38 (C-7), 44.96 (benzylamine CH₂). HRMS-ESI(-) (C₁₈H₁₄N₅) [M-H]⁻ m/z calcd 300.1255, found 300.1243.

Data for **12f**: Yield 40%, brown solid m.p.: 222-223°C (ether), ¹H NMR (600 MHz, DMSO-*d*₆) δ 8.67 (d, $J = 5.8$ Hz, 2H, pyridinyl H-3,5), 7.90 (d, $J = 5.5$ Hz, 1H, H-5), 7.69 (d, $J = 5.8$ Hz, 2H, pyridinyl H-2,6), 7.25 (t, $J = 7.4$ Hz, 2H, benzyl H-3,5), 7.20 (t, $J = 7.2$ Hz, 1H, benzyl H-4), 6.98 (d, $J = 7.5$ Hz, 2H, benzyl H-2,6), 6.59 (s, 2H, NH₂), 6.46 (d, $J = 5.5$ Hz, 1H, H-6), 5.62 (s, 2H, benzyl CH₂). ¹³C NMR (151 MHz, DMSO-*d*₆) δ 150.10 (pyridinyl C-3,5), 149.16 (C-2), 147.18 (C-3a), 146.56 (C-7), 145.77 (C-5), 137.68 (pyridinyl C-1), 137.25 (benzyl C-1), 128.66 (benzyl C-3,5), 127.35 (benzyl C-4), 126.20 (benzyl C-2,6), 122.80 (C-7a), 122.57 (pyridinyl C-2,6),

102.81 (C-6), 45.83 (benzyl CH₂). HRMS-ESI(+) (C₁₈H₁₆N₅) [M+H]⁺ m/z calcd 302.1400, found 302.1408.

4.2 Aspergillus manipulations. Standard complete and minimal media (MM) for *A. nidulans* were used. Media and supplemented auxotrophies were at the concentrations given in <http://www.fgsc.net>. 10 mM, NaNO₃ was used as a nitrogen source. Inhibitors are added in MM dissolved in DMSO at 500 μM. Transformations were performed as described previously. Strains have been described before.^{20,23} In brief, the three strains used each expressed either FcyB, or AzgA or UapA, in an otherwise isogenic genetic background that lacked, due to total deletions of the corresponding genes, any other nucleobase-nucleoside-allantoin transporter (*uapAΔ uapCΔ azgAΔ furDΔ furAΔ fcybΔ cntA*). The transporter to be studied in each case was introduced by standard genetic transformation²⁴ with a plasmid carrying the corresponding gene expressed by its native promoter.

4.3 Transport assays. Transport assays for measuring the activity of purine transporters, such as FcyB, AzgA or UapA, is carried out in germinating conidiospores, as recently described in detail by Kryptou and Diallinas.[22] For transport competition assays, 0.5 μM of ³H-radiolabelled substrate (adenine or xanthine) is added in a mix with 1000-fold excess analogues (500 μM). Assays are terminated by freezing, immediate centrifugation and washing of cells. K_i values are estimated from IC₅₀ measurements using the Cheng and Prusoff equation [K_i = IC₅₀/1+ [S]/K_m, where [S] is the fixed concentration of radiolabeled substrate used] and analyzed by the GraphPad Prism software. All experiments are carried out at three times, with each assays performed in triplicate. Standard deviation in all cases is less than 30%. Radiolabeled purines used are: [2,8-³H]-adenine or [8-³H]-xanthine 22.8 Ci/mmol, all from Moravek Biochemicals.

4.4 Homology Modeling. The 3D Model of Fcyb was constructed based on the crystal structure of bacterial benzyl-hydantoin Mhp1 transporter (PDB entry 4D1D)[13] and we utilized the alignment already published by our group.[7] The final model was built using Prime software (Schrodinger Release 2017-4: Prime, Schrödinger, LLC, New York, NY, 2017) and the resulted model was prepared using the Protein Preparation Wizard as implemented on Maestro 10 (Schrödinger Release 2017-4: Schrödinger Suite 2017-4 Protein Preparation Wizard; Epik, Schrödinger, LLC, New York, NY, 2017; Impact, Schrödinger, LLC, New York, NY, 2017; Prime, Schrödinger, LLC, New York, NY, 2017).

4.5 Docking calculations.

4.5.1. Ligand and Protein Preparation. All analogues designed were prepared using the ligand preparation wizard as implemented in Maestro 10 (Schrödinger Release 2017-4: LigPrep, Schrödinger, LLC, New York, NY, 2017).

4.5.2. Induced Fit Docking. Schrödinger developed and validated an Induced Fit Docking protocol based on Glide and the Refinement module in Prime for accurate prediction of ligand binding modes and concomitant structural changes in the receptor. (Schrödinger Release 2017-4: Schrödinger Suite 2017-4 Induced Fit Docking protocol; Glide, Schrödinger, LLC, New York, NY, 2016; Prime, Schrödinger, LLC, New York, NY, 2017).[25] The IFD protocol models induced fit docking of ligands using the following steps:

1. An optional constrained minimization of the receptor (protein preparation, refinement only) with an RMSD cutoff of 0.18 Å. Normally this is done when preparing the protein with the Protein Preparation Wizard.

2. Initial Glide docking of each ligand using a softened potential (van der Waals radii scaling), and optional removal of side chains and application of constraints. By default, a maximum 20 poses per ligand are retained, and by default poses to be retained must have a Coulomb-vdW score less than 100 and an H-bond score less than -0.05.
3. Prime side-chain prediction for each protein-ligand complex, on residues within a given distance of any ligand pose (default 5 Å), with optional inclusion or exclusion of other residues, and an optional implicit membrane model.
4. Prime minimization of the same set of residues and the ligand for each protein/ligand complex pose. The receptor structure in each pose now reflects an induced fit to the ligand structure and conformation.
5. Glide redocking of each protein-ligand complex structure within a specified energy of the lowest-energy structure (default 30 kcal/mol). The ligand is now rigorously docked, using default Glide settings, into the induced-fit receptor structure.
6. Estimation of the binding energy (IFDScore) for each output pose.

4.6. Molecular Dynamics Simulations. Molecular Dynamic simulations were conducted with Desmond v.3 software (Schrödinger Release 2017-3: Desmond Molecular Dynamics System, D. E. Shaw Research, New York, NY, 2017. Maestro-Desmond Interoperability Tools, Schrödinger, New York, NY, 2017.).[26] First the system was prepared by embedding the protein in a POPC lipid bilayer, solvating the membrane by TIP3P explicit water, neutralizing with counter ions and adding 150 mM salt. Initially a stepwise equilibration protocol was utilized, developed by Desmond for membrane proteins. A 90 ns simulation was performed in the NPT ensemble with Langevin thermostat and barostat and semi isotropic pressure restraints for the substrate studied (compound **10a**). All figures were created with Maestro v10 (Schrödinger Release 2017-4: Maestro, Schrödinger, LLC, New York, NY, 2017).

ACKNOWLEDGEMENTS

This research was co-supported by the European Union (European Social Fund) and Greek national funds through the Operational Program “Education and Lifelong Learning” of the National Strategic Reference Framework-Research Funding Program: THALES, investing in knowledge society through the European Social Fund. G. Papadaki was supported by a “Stavros Niarchos Foundation” fellowship within the framework of a research grant to the National and Kapodistrian University of Athens.

SUPPLEMENTARY DATA

The Supplementary Data contains the ¹H-NMR and ¹³C-NMR spectra of synthesized compounds, and Supplementary Figure SF1 related to the MD simulations.

REFERENCES

- [1] Darlington, A. J., and Scazzocchio, C. (1967) Use of Analogues and the Substrate-Sensitivity of Mutants in Analysis of Purine Uptake and Breakdown in *Aspergillus nidulans*, *Journal of Bacteriology* 93, 937-940.
- [2] Diallinas, G., and Scazzocchio, C. (1989) A gene coding for the uric acid-xanthine permease of *Aspergillus nidulans*: inactivational cloning, characterization, and sequence of a cis-acting mutation, *Genetics* 122, 341.

- [3] Pantazopoulou, A., and Diallinas, G. (2007) Fungal nucleobase transporters, *FEMS Microbiology Reviews* 31, 657-675.
- [4] Diallinas, G., and Gournas, C. (2008) Structure-function relationships in the nucleobase-ascorbate transporter (NAT) family: lessons from model microbial genetic systems, *Channels (Austin, Tex.)* 2, 363-372.
- [5] Gournas, C., Papageorgiou, I., and Diallinas, G. (2008) The nucleobase-ascorbate transporter (NAT) family: genomics, evolution, structure-function relationships and physiological role, *Molecular BioSystems* 4, 404.
- [6] Kryptou, E., Lambrinidis, G., Evangelidis, T., Mikros, E., and Diallinas, G. (2014) Modelling, substrate docking and mutational analysis identify residues essential for function and specificity of the major fungal purine transporter AzgA, *Molecular Microbiology* 93, 129-145.
- [7] Kryptou, E., Kosti, V., Amillis, S., Myrianthopoulos, V., Mikros, E., and Diallinas, G. (2012) Modeling, Substrate Docking, and Mutational Analysis Identify Residues Essential for the Function and Specificity of a Eukaryotic Purine-Cytosine NCS1 Transporter, *Journal of Biological Chemistry* 287, 36792-36803.
- [8] Sioupouli, G., Lambrinidis, G., Mikros, E., Amillis, S., and Diallinas, G. (2017) Cryptic purine transporters in *Aspergillus nidulans* reveal the role of specific residues in the evolution of specificity in the NCS1 family: Cryptic purine transporters in *A. nidulans*, *Molecular Microbiology* 103, 319-332.
- [9] Hamari, Z., Amillis, S., Drevet, C., Apostolaki, A., Vágvölgyi, C., Diallinas, G., and Scazzocchio, C. (2009) Convergent evolution and orphan genes in the Fur4p-like family and characterization of a general nucleoside transporter in *Aspergillus nidulans*, *Molecular Microbiology* 73, 43-57.
- [10] Kryptou, E., Evangelidis, T., Bobonis, J., Pittis, A. A., Gabaldón, T., Scazzocchio, C., Mikros, E., and Diallinas, G. (2015) Origin, diversification and substrate specificity in the family of NCS1/FUR transporters: Origin and specificity of Fur transporters, *Molecular Microbiology* 96, 927-950.
- [11] Lu, F., Li, S., Jiang, Y., Jiang, J., Fan, H., Lu, G., Deng, D., Dang, S., Zhang, X., Wang, J., and Yan, N. (2011) Structure and mechanism of the uracil transporter UraA, *Nature* 472, 243-246.
- [12] Shimamura, T., Weyand, S., Beckstein, O., Rutherford, N. G., Hadden, J. M., Sharples, D., Sansom, M. S. P., Iwata, S., Henderson, P. J. F., and Cameron, A. D. (2010) Molecular Basis of Alternating Access Membrane Transport by the Sodium-Hydantoin Transporter Mhp1, *Science* 328, 470-473.
- [13] Simmons, K. J., Jackson, S. M., Brueckner, F., Patching, S. G., Beckstein, O., Ivanova, E., Geng, T., Weyand, S., Drew, D., Lanigan, J., Sharples, D. J., Sansom, M. S., Iwata, S., Fishwick, C. W., Johnson, A. P., Cameron, A. D., and Henderson, P. J. (2014) Molecular mechanism of ligand recognition by membrane transport protein, Mhp1, *The EMBO Journal* 33, 1831-1844.
- [14] Weyand, S., Shimamura, T., Yajima, S., Suzuki, S., Mirza, O., Krusong, K., Carpenter, E. P., Rutherford, N. G., Hadden, J. M., O'Reilly, J., Ma, P., Saidijam, M., Patching, S. G., Hope, R. J., Norbertczak, H. T., Roach, P. C. J., Iwata, S., Henderson, P. J. F., and Cameron, A. D. (2008) Structure and Molecular Mechanism of a Nucleobase-Cation-Symport-1 Family Transporter, *Science* 322, 709-713.
- [15] Yu, X., Yang, G., Yan, C., Baylon, J. L., Jiang, J., Fan, H., Lu, G., Hasegawa, K., Okumura, H., Wang, T., Tajkhorshid, E., Li, S., and Yan, N. (2017) Dimeric structure of the uracil:proton symporter UraA provides mechanistic insights into the SLC4/23/26 transporters, *Cell Research* 27, 1020-1033.

- [16] Alguel, Y., Amillis, S., Leung, J., Lambrinidis, G., Capaldi, S., Scull, N. J., Craven, G., Iwata, S., Armstrong, A., Mikros, E., Diallinas, G., Cameron, A. D., and Byrne, B. (2016) Structure of eukaryotic purine/H⁺ symporter UapA suggests a role for homodimerization in transport activity, *Nature Communications* 7, 11336.
- [17] Diallinas, G. (2014) Understanding transporter specificity and the discrete appearance of channel-like gating domains in transporters, *Frontiers in Pharmacology* 5.
- [18] Diallinas, G. (2016) Dissection of Transporter Function: From Genetics to Structure, *Trends in Genetics* 32, 576-590.
- [19] Alguel, Y., Cameron, A. D., Diallinas, G., and Byrne, B. (2016) Transporter oligomerization: form and function, *Biochemical Society Transactions* 44, 1737-1744.
- [20] Lougiakis, N., Gavriil, E.-S., Kairis, M., Sioupouli, G., Lambrinidis, G., Benaki, D., Kryptou, E., Mikros, E., Marakos, P., Pouli, N., and Diallinas, G. (2016) Design and synthesis of purine analogues as highly specific ligands for FcyB, a ubiquitous fungal nucleobase transporter, *Bioorganic & Medicinal Chemistry* 24, 5941-5952.
- [21] Yin, X., and Schneller, S. W. (2004) L-deaza-5'-noraisteromycin, *Nucleosides, Nucleotides & Nucleic Acids* 23, 67-76.
- [22] Kryptou, E., and Diallinas, G. (2014) Transport assays in filamentous fungi: kinetic characterization of the UapC purine transporter of *Aspergillus nidulans*, *Fungal Genet Biol* 63, 1-8.
- [23] Shivakumar, D., Williams, J., Wu, Y., Damm, W., Shelley, J., and Sherman, W. (2010) Prediction of Absolute Solvation Free Energies using Molecular Dynamics Free Energy Perturbation and the OPLS Force Field, *Journal of Chemical Theory and Computation* 6, 1509-1519.
- [24] Koukaki, M., Giannoutsou, E., Karagouni, A., and Diallinas, G. (2003) A novel improved method for *Aspergillus nidulans* transformation, *Journal of Microbiological Methods* 55, 687-695.
- [25] Sherman, W., Day, T., Jacobson, M. P., Friesner, R. A., and Farid, R. (2006) Novel procedure for modeling ligand/receptor induced fit effects, *J Med Chem* 49, 534-553.
- [26] Shivakumar, D., Williams, J., Wu, Y., Damm, W., Shelley, J., and Sherman, W. (2010) Prediction of Absolute Solvation Free Energies using Molecular Dynamics Free Energy Perturbation and the OPLS Force Field, *Journal of Chemical Theory and Computation* 6, 1509-1519.

Structure-activity relationships in fungal nucleobases transporters as dissected by the inhibitory effects of novel purine analogues

Efthymios-Spyridon Gavriil,^a Spyridon Dimitrakis,^a Georgia Papadaki,^b Sophia Balaska,^b George Lambrinidis,^a Nikolaos Lougiakis,^a Panagiotis Marakos,^a George Diallinas^{*,b}, Nicole Pouli,^a Emmanuel Mikros^{*,a}

Highlights

- Rationally designed 3-deazapurine analogues are synthesized and used in studying transporter-ligand interactions
- Novel 3-deazaxanthine analogues are recognized by a single (FcyB) or multiple (FcyB and AzgA) fungal transporters
- Active compounds stabilize the outward transporter conformation.
- Fungal purine transporters can be used as specific gateways for the design of highly targeted novel antifungals or drug cocktails